Lidar Detection of Moored Mines

René CARMONA,[*] and Lixin WANG[†]
Department of Operations Research & Financial Engineering,
Princeton University, Princeton, NJ 08544

September 17, 2000

Abstract

In this paper, we present a set of new image processing algorithms for moored mines detection. Data from the Magic Lantern Development Contingency (ML(DC)) system are used for illustration purposes. The main ingredients of our detection algorithm are a reduction to binary images and processing by morphological operations. The results obtained on the ML(DC) data are very promising: the detection rate is optimal and the false alarm rate is very low. Moreover the algorithm is simple enough for real time implementations to be possible.

1 Introduction

Moored mines represent an important low-tech and inexpensive threat to the safety of the Navy ships and landing crafts. For these reasons, and because of its implications to marine life protection, the clearance of sea-mines has gained nationwide support and international attention in recent years. Recent improvements in computational power together with technological advances in remote sensing devices should enable the development of reliable real-time sea-mines identification and detection image processing tools. The present paper is a contribution to the latter. See [4] and the references therein, for existing work on the same topic.

In 1995, a database of sea mine and minefield reconnaissance images was collected by the Navy using the Magic Lantern (ML) system. This database was designed to assist the development of automatic target recognition (ATR) algorithms. Two main systems are used in the collection of sea mine images: the Magic Lantern Development Contingency

[*] Partially supported by ONR grant N00178-99-1-9003 and N00178-00-1-9001

[†] Supported by ONR grant N00178-00-1-9001

(ML(DC)) system for moored sea mines, and the Magic Lantern Adaptation (ML(A)) system for mines in the surf zone. Our work focuses on the detection of moored sea-mines in deep water from an airborne platform, so we work with images from the ML(DC) system. The main environmental factors influencing the imaging processing are the water clarity and sea state: they affect the light propagation and they severely distort the target images, making the detection difficult. Our previous work [5] contains an in depth analysis of the image degradation process, but unfortunately, it is not possible to use it in the present analysis. Indeed, our main concern is the detection of the mines (and the mine like objects), and since the flying altitude of the helicopter was much higher in the ML(DC) experiment, the size of the mines is not greater than 15 pixels on the average, and there is no way to take advantage of the image degradation phenomenon identified and studied in [5].

In the following section, we describe the relevant features of the ML(DC) data provided by the Navy, and which we use as a testbed for our detection algorithm. Because of the elevation at which the imaging platform is flying, it appears that, when present in the images, the mines affect a small number of pixel values. So, to counteract distortion effects of this nature, our experiments suggest that the use of morphological operations is best suited. Using standard image processing procedures and repeated erosions and/or dilations, we process the original ML(DC) images into objects with an over simplified structure. Then we quantify the statistical features of these objects, such as the areas and the locations of the centroids. The final detection algorithm is based on a set of decision rules involving these empirical statistics. Since we only had access to unclassified data, we did not have information on the *ground truth* about which images contained mines, and what kind of mine they were. So not only were we unable to consider the classification problem, but our detection rules had to be designed and tested from *best guess computations* based on the mine field map and the flying parameters disclosed in the ML(DC) released documentation.

The paper is organized as follows. In Section 2, a description of the ML(DC) data is given. In Section 3, we introduce the morphological operations used in this study. We state the notation, and we review the terminology and the definitions of the operations entering in our pre-processing of the ML(DC) data. We provide the details of our preprocessing procedure in Section 4. It consists of two main steps: image enhancement and morphological processing. Then we explain the rationale of the decision rules entering the detection algorithm, and we illustrate their implementation on the enhanced images. Experimental results are reported in Section 6.

2 The ML(DC) Data Set

The Magic Lantern Development Contingency (ML(DC)) system is a ranged-gated light detection and ranging (LIDAR) system, consisting of three main optical subsystems: the scanner, the laser and a set of six imaging receivers. It is worth mentioning that the six imaging receivers are adjusted to six overlapping gates. This design was chosen to maximize the chance of correct detection and identification of the mines. Table 2 gives a typical configuration for the numerical settings of these gates.

camera#	Receiver Gated Settings
1	12-32 ft
2	16-36 ft
3	20-40 ft
4	25-40 ft
5	35-45 ft
6	40-50 ft

Table 1: Depth Gate Settings for each Camera for ML(DC)

We refer the reader interested in further details on the ML(DC) system to the report [2]. For the purpose of the present study, the images collected from these six gates will be called tiles, and they will be reproduced side by side, from left to right when we increase the depth of the gate. See Figures 1 and 2 for examples of two tilings. Our expectation is that, if a mine (or a mine like object) is present at a depth covered by one of the gate settings, one should observe a bright spot in the corresponding tile, due to the reflection of the light rays at the object surface. Moreover, because of the shadow cast by the object obstruction to the light propagation, we should also expect dark spots in the tiles corresponding to the gates below the object. These phenomena have been documented and implemented in our simulation study reported in [5]. But, contrary to the simulations produced in [5], the proportion of the image occupied by the mines appear to be much smaller, and this will dramatically affect our detection strategy. Indeed, the size of the mines which identifed for the purpose of this detection study, varies from 4 pixels to 36 pixels. This is caused by the flying altitude of the helicopter, which we roughly estimate at approximately 500 ft on the average. Under these conditions, it is not possible to use the degradation process modeled and simulated in [5] as a basis for our detection algorithm.

The data used in this study are from the June 1995 ML(DC) Flight Verification Test conducted in the Gulf of Mexico, off the coast of Panama City. Figures 1 and 2 give two sample tilings.

Figure 1, was chosen because it shows clearly the expected signature of a mine: we see a bright spot in the first tile, nothing significant in the second, and dark shadows in the tiles corresponding to the remaining gates. Referring to the settings given in Table 2, one can infer that the depth of the mine is between 12ft and 20ft.

Figure 2 gives an example of a tiling where it is difficult to identify any region with bright or shady parts in the individual tiles. We suspect that there is no mine in the vertical

Figure 1: Typical tiling of images of a gated region containing a mine.

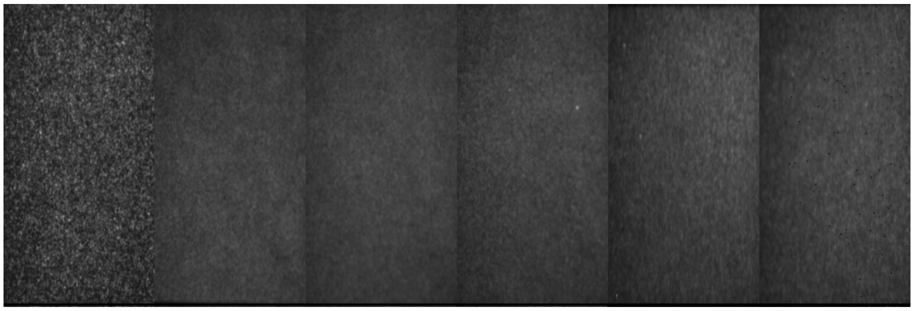

Figure 2: Typical tiling if images of a gated region without any mine.

water column imaged in this tile.

As a final remark, we notice the lack of contrast in most of the images of the tilings containing a mine. There is no doubt that this ought to be a serious hindrance to any detection attempt. To alleviate this problem, we propose an enhancement procedure in Section 4. But before we can discuss the elements entering this pre-processing of the images, we need to review the notation and basics of binary morphological operations.

3 Binary Morphological Operations

The first step of our pre-processing strategy will produce tilings comprising binary images which hopefully capture the main mine features. The second step will rely on binary morphological operations to further enhance the salient features of the mines. For the sake of completeness, we review the definitions of the binary morphological operations used in this study.

Binary morphological operations are tools designed to operate on subsets of a given set with an additive structure. These operations can be implemented in the context of binary images with pixel values 0 and 1, as long as the subsets involved in the operations are identified with the sets of pixels with value 1. In general, the structure of a morphological operation involves three elements: the original binary image A, a structuring element B, and the operator itself. The most basic operators are dilation and erosion. We review them first.

3.1 Erosion and Dilation

Let A be a binary image, and let B be a binary structuring element. The latter is nothing but a subset containing the zero of the additive structure. The operator of dilation, $\oplus$, is defined on A and B by he formula:

$$A \oplus B = \{a + b | a \in A, b \in B\}.$$

$A \oplus B$ is called the dilation of A by B. This operation is obviously commutative in the sense that $A \oplus B = B \oplus A$. The result $A \oplus B$ is sometimes called the Minkowski sum of the sets A and B. *Note that we assume that the structuring element includes the origin.* Notice that:

$$A \subset A \oplus B.$$

Similarly, the erosion of A by B is defined by the formula:

$$A \ominus B = \{h | B_h \subseteq A\},$$

where $B_h = \{b + h | b \in B\}$ denotes the shift of the set B by the pixel element h. It is easy to see that the shift satisfies:

$$A_h \ominus B = A \ominus B_h = (A \ominus B)_h,$$

Unlike dilation, erosion is not commutative. The following formulae give some of the important properties of the dilation and erosion operations which help explain their nature and how we will use them. First the dilation satisfies:

$$\begin{aligned}
&A_h \oplus B = A \oplus B_h = (A \oplus B)_h, \\
&A \oplus B \subseteq A \oplus C \quad \text{whenever} \quad B \subseteq C, \\
&A \oplus (B \cup C) = (A \oplus B) \cup (A \oplus C), \\
&A \oplus (B \cap C) = (A \oplus B) \cap (A \oplus C).
\end{aligned}$$

Next the erosion operation satisfies:

$$\begin{aligned}
&A \ominus B \supseteq A \ominus C \, if \; B \subseteq C, \\
&A \ominus (B \cup C) = (A \ominus B) \cap (A \ominus C), \\
&A \ominus (B \cap C) = (A \ominus B) \cup (A \ominus C).
\end{aligned}$$

3.2 Opening and Closing

Dilation and erosion are the basic building blocks used in the construction of elaborated operations. We shall limit ourselves to two of the simplest ones: opening and closing. The opening of A by B is defined by the formula:

$$A \circ B = (A \ominus B) \oplus B,$$

in other words, A is first eroded by B and subsequently dilated by B. The resulting binary image is smaller than A, i. e. $A \circ B \subseteq A$. If we change the order of the operations of erosion and dilation, we obtain what is called the closing of A by B:

$$A \bullet B = (A \oplus B) \ominus B.$$

This time the result is a larger set since $A \subseteq A \bullet B$. As before, we list the most important properties of the openings:

$$\begin{aligned}
&A \subseteq B \Rightarrow A \circ C \subseteq B \circ C, \quad \text{(increasing property)}\\
&A \circ B \subseteq A, \quad \text{(anti-extensive property)}\\
&(A \circ B) \circ B = A \circ B. \quad \text{(idempotent property)}
\end{aligned}$$

and of the closings:

$$\begin{aligned}
&A \subseteq B \Rightarrow A \bullet C \subseteq B \bullet C, \quad \text{(increasing property)}\\
&A \subseteq A \bullet B, \quad \text{(extensive property)}\\
&(A \bullet B) \bullet B = A \bullet B. \quad \text{(idempotent property)}
\end{aligned}$$

Openings and closings are useful to remove the so-called *pepper* and *salt* noises. We shall use them extensively in our study. We refer the interested reader to Heijmans' book [1] for details and complements.

4 Pre-Processing on the Raw Data

The ML(DC) data comprise a large number of 8-bits digital images with 256 rows and 168 columns. As explained earlier, these images are grouped in sets of 6 images which we call tilings. Each tiling carries information on the water column over a given rectangle at the surface.

As we mentioned at the end of Section 2, the poor contrast between the patch of pixels covering a mine location and its surrounding neighborhood, is a serious obstacle to the detection of the mine. It would be nice if we could exacerbate the intensity difference between these two regions as a preparation for the detection stage. This is one of the several treatments of the image tiles designed to enhance the images before we address the actual detection issues. There are two major components in our pre-processing algorithm: image enhancement and morphological processing. We discuss them separately.

4.1 Image Enhancement

In turn, the enhancement of the individual image tiles is also done in two steps.

Linear Stretch

Most of the images have a small dynamic range: they do not use the full 256 gray level scale. Therefore, we first stretch the range of the image linearly to the full range by the transformation taking an image I into the image $\overline{I}$ defined by:

$$\overline{I(i,j)} = 255 \times \frac{I(i,j) - I_{min}}{I_{max} - I_{min}},$$

where $i = 1, \dots, 256$ and $j = 1, \dots, 168,$ are the pixel coordinates, and $I_{max},\ I_{min}$ are the maximum and minimum gray levels appearing in the image I.

Histogram Clipping

After linearly stretching the image to the full gray level range, we still need to increase the contrast between the target and its background. To this end, we use the standard histogram clipping technique. The idea of histogram clipping is to find the new I_{max} and I_{min}, such that the corresponding histogram bins are the first ones above a given threshold from the upper end 255, and the low gray level 1 respectively. In our case, the threshold is set to $0.01\% \times 256 \times 168$. Then clip those pixel values greater than the new I_{max} to I_{max}, less than the new I_{min} to I_{min}. Finally we linearly stretch the image back to the full range $[0, 255]$.

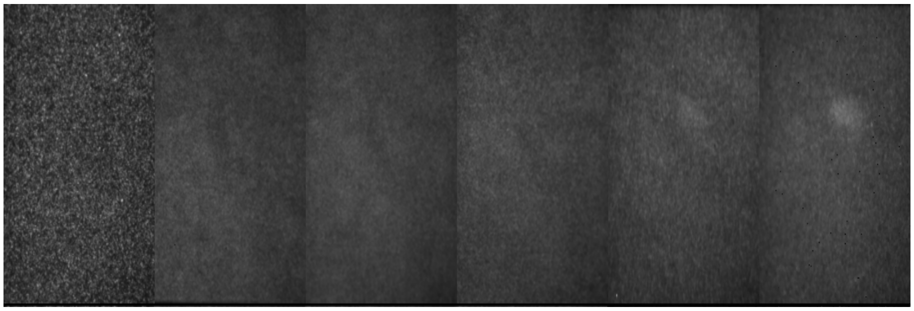

Figure 3: A raw image.

Figures 3 and 4 illustrate our enhancement procedure. Figure 3 shows a raw tiling and Figure 4 shows the tiling after the enhancement procedure which we just described. This special tiling was chosen because it contains a mine like object in the fifth and sixth gates, and while this mine is difficult to see in the raw images reproduced in the tiling of Figure 3, it becomes obvious in the enhanced tiling: after processing we can tell the target from its background much easier.

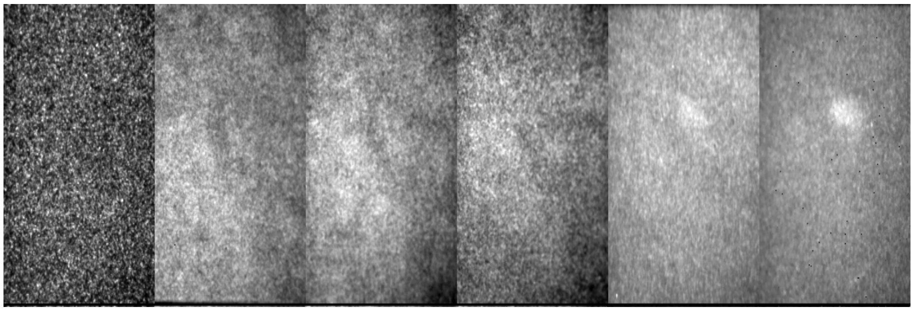

Figure 4: The enhanced image.

4.2 Morphological Processing on the Enhanced Image

Mines and mine-like objects appear in the tilings as compact bright spots and/or shadows depending on their depths. Since we mainly aim at finding this salient feature, we shall threshold the gray level images to transform them into binary images amenable to morphological processing. The thresholding is done differently for shadow and bright spot captures.

Shadow Extraction

The shadow of a mine is a region of the image characterized by intensity differences with its local background following a specific pattern. In order to identify the mine shadows we use the following procedure. For each pixel $(i, j) \in I$, we compute the local average $\mu_s(i, j; I)$ as the mean pixel level over the 3×3 square centered around the pixel (i, j), and the local average $\mu_b(i, j; I)$ over the 35×35 square with the same center. We adjust for boundary effects when the pixel (i, j) is near the boundary of the image. Then we compute the standard deviations $\sigma_s(i, j; I)$ and $\sigma_b(i, j; I)$ of the pixel values in these neighborhoods of the pixel (i, j). We then compute the contrast difference at pixel (i, j) as the quantity:

$$CD(i, j) = \mu_b(i, j; I) - \mu_s(i, j; I).$$

Our thresholding procedure goes as follows: if this difference $CD(i, j)$ is smaller than $2.0 \times \sqrt{\sigma_b(i, j; I) + \sigma_s(i, j; I)}$, the value of the pixel (i, j) is clipped to 0. Otherwise we set it to one. In this way, we get a binary image. Given this binary image, the search for a shadow continues with a binary morphological operation. We perform a closing followed by an opening, with the discrete *RHOMBUS* structuring element B defined by:

$$B = \begin{pmatrix} 0 & 1 & 0 \\ 1 & 1 & 1 \\ 0 & 1 & 0 \end{pmatrix}.$$

Bright Spot Extraction

The bright spots of an image are detected by a procedure which relies on two separate attempts at achieving the same goal.

Firstly, we try to identify the parts of the images where the intensity is very high in a very traditional way. This is motivated by our preliminary observations which indicate that mines appear as bright spots in the images corresponding to the gates containing the mines. For a given image A, we compute the 98.5 percentile of the gray levels in the image, and we set to 1 the pixels with a level higher than this percentile, and to 0 the remaining pixels. Next, we *smooth* the binary image by a closing and an opening with the structuring element B defined by the matrix:

$$B = \begin{pmatrix} 1 & 1 & 1 & 1 & 1 \\ 1 & 1 & 1 & 1 & 1 \\ 1 & 1 & 1 & 1 & 1 \\ 1 & 1 & 1 & 1 & 1 \\ 1 & 1 & 1 & 1 & 1 \end{pmatrix}.$$

We call the resulting image A_1.

Secondly, we use the statistical discrimination method used before to identify the shadows. We apply it to the *negative image* A' obtained by replacing each pixel value $A(i,j)$ by $A'(i,j) = 255 - A(i,j)$. As before, we identify the pixels where there is a significant difference between the two local averages around the pixels. This time, we use the structuring element B given by the matrix:

$$B = \begin{pmatrix} 1 & 1 & 1 \\ 1 & 1 & 1 \\ 1 & 1 & 1 \end{pmatrix}.$$

In this way, we obtain another binary image A_2, and the final binary image $\overline{A}$ which we regard as the result of the bright spot extraction is obtained by combining A_1 and A_2 in a binary addition:

$$\overline{A} = A_1 \cup A_2.$$

5 Mine Detection in a Tiling

The ML(DC) imaging system provides sets of six sub-images (each sub-image corresponding to a gate) which we referred to as tilings. When a mine (or mine like object) is present in a tiling, the transition between two successive sub-images of the tiling follows one of the following three patterns, depending on the relative values of the depth of the mine and the gate ranges of the sub-images:

1. *bright spot* → *bright spot* whenever the overlap between the two consecutive gates contains the mine,
2. *bright spot* → *shadow* whenever the mine is in the range of the first gate and not of the second,
3. *shadow* → *shadow* whenever the mine is above the gates of the two sub-images.

Our detection algorithm is designed to identify these three transition patterns. This identification is based on the numerical statistics which we introduce in the next subsection. The following subsections are devoted to the identification of these transitions from the values of these statistics.

Computations of these statistics the last section, we extract the bright or shadow region from the image. Thus we can implement the detection algorithm on these binary images. First we compute the statistical features(image area and centroid) on the images. Then we use three functions to tell if the target appears in one of the three patterns: we say there is a mine in the tile if one of the functions provides the positive answer; otherwise there is no mine.

5.1 Statistics of the Binary Tiles

The statistical features used in the detection procedure are based on the notion of centroid of a sub-image as defined as follows.

As explained earlier, a mine (or mine like object) appears in a tile as a bright spot or a shadow. So, each tiling is processed twice, once for the bright spots and once for the shadows.

1) We process each of the six sub-images of a given tiling with the bright spot identification algorithm described in the previous section. In each sub-image we keep only the two largest connected components of bright pixels (those pixels set to 1 by the algorithm), and we compute their areas. Next, we compute the coordinates of the centroids of those components whose areas are greater than a preset value (we used the value of 25 pixels in our experiments). In this way, we produce a 6×4 matrix, each row being either empty, or containing the coordinates of the centroid of a bright spot, or the coordinates of two such bright spots.

2) Next we process the tiling for shadows. We use the shadow identification algorithm described in the previous section on each sub-images. We follow the same steps as for the search for bright spot centroids, except for the fact that we set the minimal area for a shadow to be 12 instead of 25. Similarly, we get a 6×4 matrix for the coordinates of the centroids of the significant shadows.

The matrices of centroid coordinates are used for detection in the following manner.

5.2 Identification of a *Bright Spot*→ *Bright Spot* Transition

The detection of a mine from a *Bright Spot*→ *Bright Spot* pattern is done in the following way. Given a tiling, we consider the matrix of bright spot centroids, and for $k = 1, \cdots, 5$, we check for the existence of a centroid in row k which is close to a centroid in one of the following rows. Specifically, for each $k = 1, \ldots, 5$, and for each of the centroids possibly present in the row of the matrix, we compute the distance with all the centroids found in the following rows $k + 1, \ldots, 6$, and if half of the distances so computed are less than a preset threshold value, we decide that there is a mine in *bright spot* → *bright spot pattern.*

Figure 5 shows the enhanced tiling where such a detection can be made. The mine appears as a bright spot in the first four tiles.brightly in most sub-images.

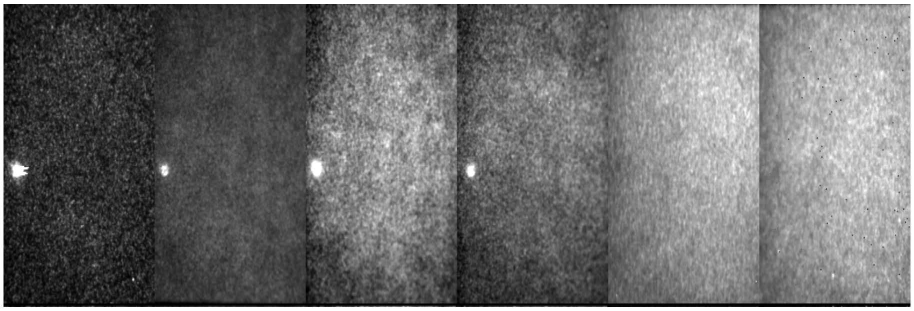

Figure 5: Enhanced tiling containing a mine in a *bright spot* → *bright spot* pattern.

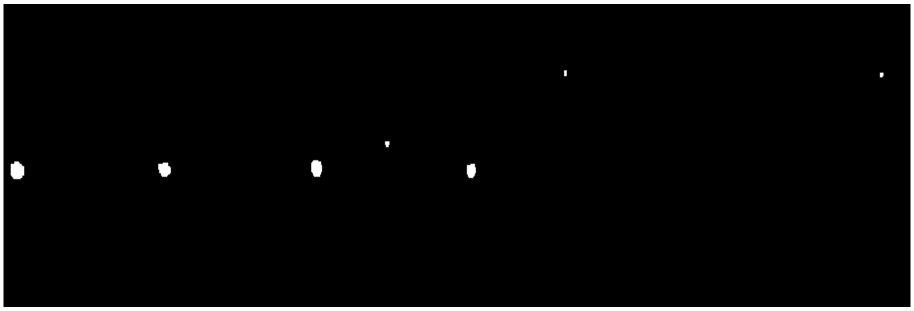

Figure 6: Bright spot extraction procedure applied to the enhanced tiling of Figure 5

Figure 6 shows the result of the bright spot extraction procedure. It is easy to guess the values of the entries of the corresponding bright spot centroid matrix. The detection algorithm does identify a mine in the *bright spot* → *bright spot* pattern at the expected location.

Figure 7 shows that the result of the shadow extraction procedure is totally uninstructive, and that the detection of the actual mine in this tiling had to be solely based on the bright spot only.

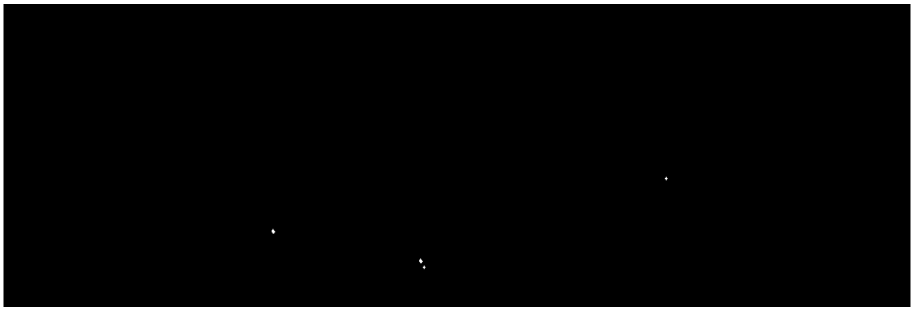

Figure 7: Shadow extraction procedure applied to the enhanced tiling of Figure 5

Remark 5.1 *It is usually possible to use the detection pattern and the gate ranges of Table 2 to give a reasonable estimate of the depth of the mine. We did not emphasize this side effect of the detection algorithm, because our main concern is the detection itself, more than the identification/classification of the target!*

5.3 Identification of a *Bright Spot* → *Shadow* Transition

In order to detect a mine in such a pattern, for each sub-image in the tiling, we check if the centroid of a bright spot does coincide with the centroid of a shadow in one of the subsequent sub-images. This is done by computing for each bright spot centroid in the k-th row of the bright spot matrix of the tiling ($k = 1, \cdots, 5$), the distances with the shadow centroids taken from the rows with index greater than k in the shadow matrix of the tiling. As before, we say that a mine is detected if half of these distances are smaller than a preset threshold. In order to illustrate this transition pattern identification we chose the tiling whose enhancement is shown in Figure 8.

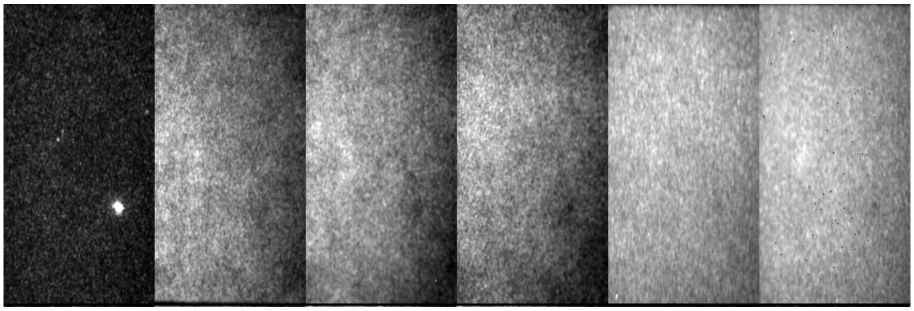

Figure 8: Enhanced tiling of a mine in a *bright spot* → *shadow* transition pattern.

The pattern exhibited by Figure 8 contains a bright spot in the first tile, and possible shadows in the last three tiles. Figures 9 and 10 showing the results of the bright spot and shadow extraction procedures confirm this first impression.

In this case, a mine in a *bright spot* → *shadow* pattern is detected by the algorithm.

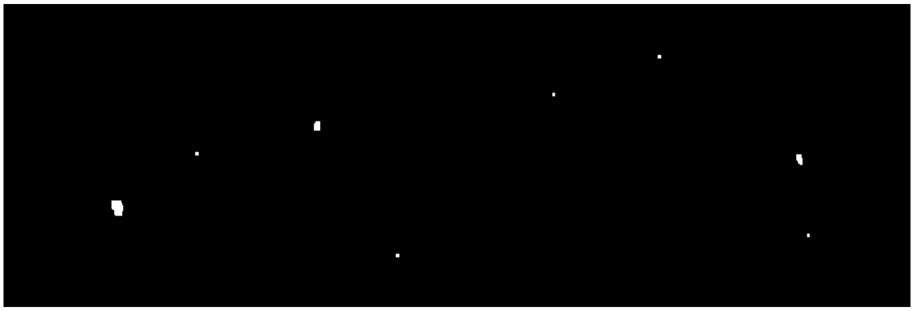

Figure 9: Bright spot extraction procedure as applied to the tiling of Figure 8

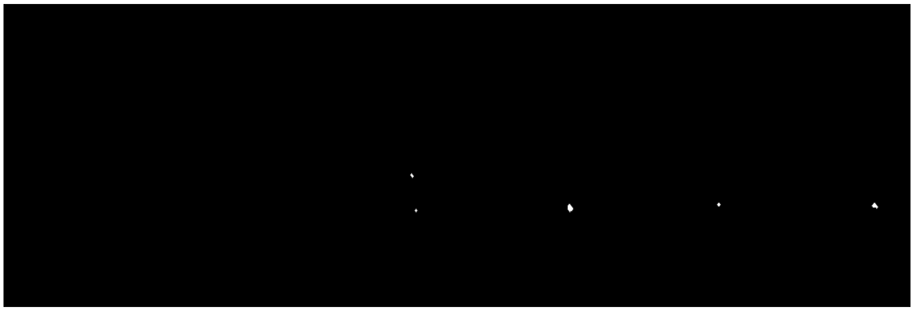

Figure 10: Shadow extraction procedure as applied to the tiling of Figure 8

5.4 Identification of a *Shadow* → *Shadow* Transition

We follow exactly the procedure detailed in Subsection 5.2 for the identification of *bright spot* → *bright spot* transitions, using the matrix of shadow centroids instead of the matrix of bright spot centroids. We illustrate the resulting decision rule with the example of the tiling whose enhanced sub-images are shown in Figure 11

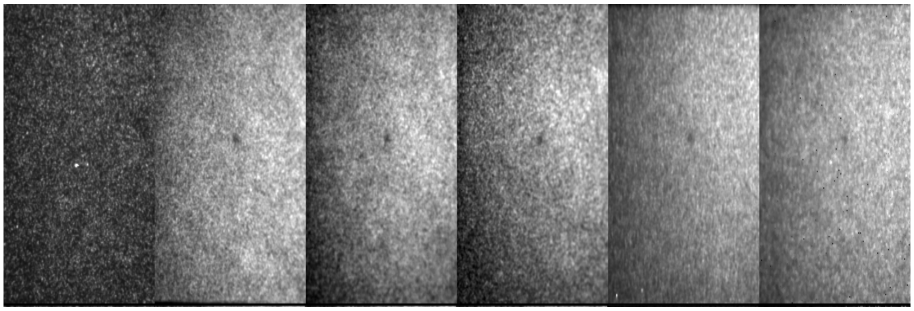

Figure 11: Enhanced tiling of a mine in a *shadow* → *shadow* pattern.

This example was selected, because the shadow of the mine appears clearly and consistently from the second sub-image to the last one. The bright spot extraction procedure gives the tiling shown in Figure 12.

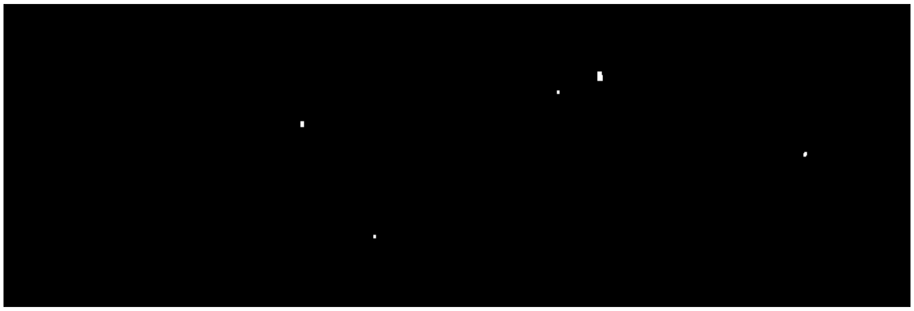

Figure 12: Bright spot extraction procedure as applied to the tiling of Figure 11

No consistent pattern appears, only noise seems to be the cause of the bright spots. The bright spot centroid matrix is empty as expected.

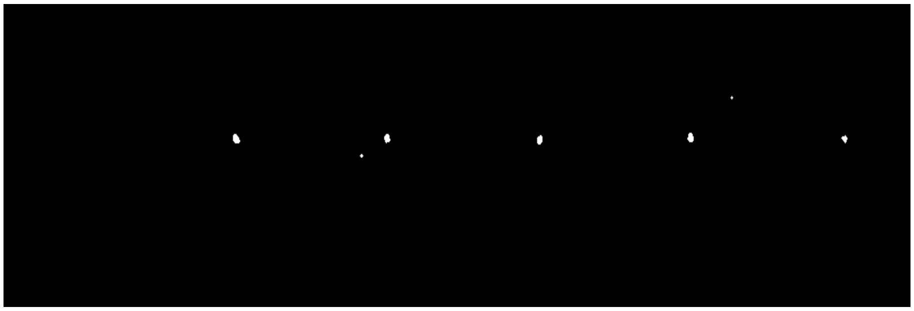

Figure 13: Shadow extraction procedure as applied to the tiling of Figure 11

On the other hand, the result of the shadow extraction reproduced in Figure 13, shows a consistent pattern of centroids, and the centroid matrix ends up as expected with an empty first row and each of the other ones containing the (essentially identical) coordinates of a centroid. The algorithm detects a mine in the *shadow* → *shadow* pattern.

6 Experimental Results

In order to test the performance of our algorithm, we applied it to some of the data files of the ML(DC) set. We used the files ”$167A2154$” and ”$170A0036$” for testing purposes, training our algorithm (to choose values for the threshold parameters) on other files. Summary information on the test files are given in Table 2:

In order to produce a ROC curve we chose to vary the distance threshold from $\sqrt{32}$ to 3, keeping all the other parameters fixed. See for example [3] for details on the generation of ROC curves. For the purpose of our ROC curves, we use the following definitions for

File#	Total Tiles	Mines	Field of View Area
167A2154	174	13	$89 \times 64\ ft^2$
170A0036	434	17	$91 \times 65\ ft^2$

Table 2: Information on the Testing Data

the *Detection Rate* and the *False Alarm Rate.*

$$\begin{aligned}\textbf{Detection Rate} &= \frac{\text{\# of mines detected}}{\text{total \# of mines in the data file}},\\ \textbf{False Alarm Rate} &= \frac{\text{\# of false alarm}}{\text{total \# of tiles with mines} \times \text{Field of View area}}.\end{aligned}$$

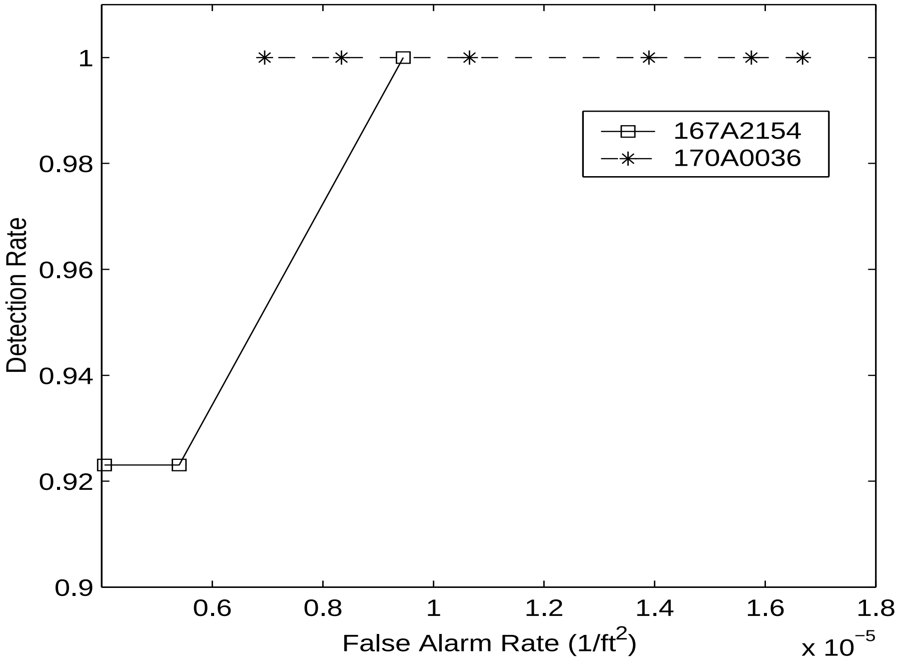

Figure 14: The ROC curves from the ”$170A0036$” and ”$167A2154$” files of the ML(DC) data set used for testing purposes.

The ROC curves show that our algorithm detects all the mines in the data file ”$170A0036$” and that for the data file ”$167A2154$”, all the mines are found with the false alarm rate not greater than 0.95×10^{-5}.

7 Conclusion

We designed an algorithm for the detection of moored mines, and we tested it in on the test files of the ML(DC) data set. The results are as good as one can expect. The next step is to test the robustness of the three major components of our algorithm: 1) the preprocessing leading to binary images, 2) their morphological treatment, and 3) the decision rules used for detection. The simplicity of the building blocks of our algorithm suggests that after thorough testing on new data sets, small perturbations of our algorithm should lead to versions with real time robust implementations.

Acknowledgements

We are grateful to Nancy Swanson for enlightening discussions on the nature, and the contents of the ML(DC) data files.

References

[1] H. Heijmans:*Morphological Image Operators*,Academic Press (1994) New York, N.Y.

[2] Costal Systems Station: *Magic Lantern (ML) Automatic Recognition (ATR) Database Report*, Jan. 1996.

[3] H. Van Trees: *Detection, Estimation, and Modulation Theory (Part I)*, John Wiley & Sons, 1968.

[4] A. J. Nevis: *Image Characterization and Target Recognition in the Surf Zone Environment*, Detection and Remediation Technologies for Mines and Minelike Targets, **2765**, SPIE, 46–57, 1996.

[5] R. Carmona, F. Cerou and B. Blasco: *Lidar Imaging of Moored Mines: a Simulation Approach*, Tech. Rep. (1999), ORFE Dept. Princeton University, Princeton, NJ.